NASA Contractor Report 187133

Elasto-Plastic Analysis of Interface Layers for Fiber Reinforced Metal Matrix Composites

I. Doghri and F.A. Leckie
University of California
Santa Barbara, California

June 1991

Prepared for
Lewis Research Center
Under Grant NAG3-894

National Aeronautics and
Space Administration

ELASTO-PLASTIC ANALYSIS OF INTERFACE LAYERS FOR FIBER REINFORCED METAL MATRIX COMPOSITES

I. DOGHRI and F.A. LECKIE

Department of Mechanical and Environmental Engineering

University of California

Santa Barbara, CA 93106

ABSTRACT

The mismatch in coefficients of thermal expansion (CTE) of fiber and matrix in metal matrix composites reinforced with ceramics fibers induces high thermal stresses in the matrix. Elasto-plastic analyses - with different degrees of simplification and modelization - show that an interface layer with a sufficiently high CTE can reduce the tensile hoop stress in the matrix substantially.

INTRODUCTION

Metal matrix composites reinforced with ceramics fibers have attractive properties for engineering applications. These composites have a high strength associated to a low density, the ceramics fibers provide a high temperature resistance, and their brittle behavior is compensated to some extent by the ductility of the metal matrix. However, because ceramics have a low coefficient of thermal expansion (CTE) and metals have a higher CTE, the induced thermal mismatch is responsible for residual stresses in the composite when subjected to a change in temperature.

Cracking in the matrix has been observed after cooling down from processing temperature to room temperature for brittle matrix materials [1]. It has been proposed that the insertion of an adequate interface layer between the fiber and the matrix can reduce the tensile stresses in the matrix to a level which avoids matrix cracking.

Some numerical parametric studies ([2], [3]) suggested that the optimum interface layer should have a CTE between those of the matrix and fiber, with a low Young's modulus and a high thickness. However, these conclusions were based on a questionable optimization procedure [2] or on limited numerical results and did not provide an understanding of the problem.

Recently, Jansson and Leckie [4] conducted a simplified analysis assuming a rigid fiber and a very thin layer. They concluded that a compensating layer with a sufficiently high CTE can reduce significantly the residual stresses in the matrix. A complete elastic analysis was performed by Doghri et al [5], who proposed an optimization procedure offering a window of candidate layer materials. Both of the two studies showed that, while the hoop stress in the matrix can be reduced substantially, the axial stress in the matrix is less affected by a layer. They also pointed out that plastic yielding may occur in the interface layer.

In this paper, plasticity is taken into account. The first part of the study is based on a three cylinder model, isolating one fiber with an interface layer and a matrix layer (Fig. 1). Only thermal loading is considered. The interface layer is elastic-perfectly plastic while the

matrix is considered either elastic or elasto-plastic. A remarkably accurate and efficient numerical procedure is developed allowing to have approximations of the stresses and strains fields everywhere in the composite.

In the second part of this study, the accuracy of the three cylinder model is investigated by studying the response of a unit cell of a hexagonal array of the fibrous composite. Finite element computations are performed under seveal thermal-mechanical loadings.

NOTATIONS

f	fiber
ℓ	layer
m	matrix
j	f, ℓ, m
R_j	external radius of j

$t_\ell = R_\ell - R_f$ layer thickness

The radii R_f and R_m are related to the fiber volume fraction C_f by $C_f = \left(\frac{R_f}{R_m}\right)^2$

E_j, ν_j	Young's modulus, Poisson's ratio of j
λ_j, μ_j	Lamé coefficients of j

$$\lambda_j = \frac{E_j \nu_j}{(1-2\nu_j)(1+\nu_j)} \quad , \quad \mu_j = \frac{E_j}{2(1+\nu_j)}$$

α_j	CTE of j
ΔT	change in temperature
σ_{rj}	radial stress (σ_{rr}) in j
$\sigma_{\theta j}$	hoop stress ($\sigma_{\theta\theta}$) in j
σ_{zj}	axial stress (σ_{zz}) in j

In the same manner, we define the total strains: $\varepsilon_{rj}, \varepsilon_{\theta j}, \varepsilon_{zj}$

and the plastic strains in the layer $\varepsilon^p_{r\ell}, \varepsilon^p_{\theta\ell}, \varepsilon^p_{z\ell}$

$\bar{\sigma}_j$	v. Mises equivalent stress in j

In the same way that the v. Mises equivalent stress is related to the distorsion energy, a so-called damage equivalent stress [6] is related to the total elastic energy and is defined by

$$\sigma^*_j = \bar{\sigma}_j \left[\frac{2}{3}(1+\nu_j) + 3(1-2\nu_j)\left(\frac{\sigma_{Hj}}{\bar{\sigma}_j}\right)^2 \right]^{1/2}$$

where $\sigma_{Hj} = (\sigma_{rj} + \sigma_{\theta j} + \sigma_{zj})/3$.

1. Development of the Stress-Strain Analysis for the Axisymmetric Thermal Problem

The composite is not subjected to transverse loading and the outer surface of the compound cylinder is traction free. The thermal loading is assumed to be axisymmetric with respect to the z-axis, so that the displacement in the transverse plane is radial: $U_j(r)$. The fibers are long and the strain and stress distributions are uniform in the z-direction except at the end regions which are not studied here. A generalized plane strain assumption is made so that ε_{zj} = constant = e_z. The other strains are given by:

$$\varepsilon_{rj} = U_j' \text{ and } \varepsilon_{\theta j} = \frac{U_j}{r}$$

and there are no shear strains.

One may use the finite element method (FEM) to solve this problem. But the problem begin axisymmetric, we developed a procedure which proved to be more flexible and much less computer time consuming than the FEM. The interface layer is assumed to be elasto-plastic while the fiber and the matrix are elastic.

We are looking for a solution which will satisfy the following conditions:

(1) The constitutive equations everywhere

(2) Exactly the equilibrium in (f) and (m)

(3) The continuity of the displacement between (f) and (ℓ) $U_f = U_\ell$ at $r = R_f$

(4) The continuity of the displacement between (ℓ) and (m) $U_\ell = U_m$ at $r = R_\ell$

(5) The stress free condition at the outer surface of the copound cylinder $\sigma_{rm} = 0$ at $r = R_m$

(6) A weak form of the equilibrium in (ℓ)

(7) The axial equilibrium condition associated with the generalized plane strain assumption $\int_0^{R_m} \sigma_{zj} r dr = 0$

This solution will not satisfy the continuity of the stress vector at the interfaces (f)/(ℓ) and (ℓ)/(m). However, it was found that the resulting jumps are not important. The iterative procedure adopted is the following:

(i) Propose a temperature increment ΔT

(ii) For the given temperature increment, propose a total strain increment in (ℓ)

- Find stresses in (ℓ) which satisfy the constitutive equations
- Find strains and stresses in (f) and (m) which satisfy the conditions (1), (2), (3), (4) and (5)
- Check if the equilibrium equations (6) and (7) are satisfied:
  - If NO, propose another strain increment in (ℓ), i.e. go to (ii)
  - If YES, for this temperature, the solution was found.

1.1 Equilibrium Conditions (6) and (7)

Any form of the total strain field in (ℓ) may be assumed, provided that the compatibility conditions are satisfied. For example, the following form of the total strains in (ℓ) is assumed

$$\varepsilon_{r\ell} = c_\ell - \left(\frac{R_\ell}{r}\right)^2 D_\ell$$

$$\varepsilon_{\theta\ell} = c_\ell + \left(\frac{R_\ell}{r}\right)^2 D_\ell$$

where c_ℓ and D_ℓ are constants to be found.

We have used the present form of the total strain field in (ℓ) because it has a uniform trace, hence the stress field has a uniform trace also and since $\varepsilon_{z\ell}$ = constant = e_z, the stress $\sigma_{z\ell}$ are likely to be almost uniform, which is in agreement with a generalized plane strain assumption.

The radial displacement is given as

$$U_\ell = c_\ell r + D_\ell \frac{R_\ell^2}{r}$$

The local equations of equilibrium in the layer are

$$\frac{\partial \sigma_{rr}}{\partial r} + \frac{1}{r}\left(\sigma_{rr} - \sigma_{\theta\theta}\right) = 0$$

We use the same procedure by which the local equations of equilibrium are extended to the global ones. We multiply the local equations by U_ℓ and integrate over the domain of (ℓ) to give:

$$\int_{R_f}^{R_\ell} \left[\frac{\partial \sigma_{rr}}{\partial r} + \frac{1}{r}\left(\sigma_{rr} - \sigma_{\theta\theta}\right)\right]\left[c_\ell r + D_\ell \frac{R_\ell^2}{r}\right] r dr = 0, \quad \forall c_\ell, \quad \forall D_\ell$$

This is a weak form of the equilibrium because we assume only a particular form of the displacement field.

The previous equation leads to the following system

$$\int_{R_f}^{R_\ell} \left[r^2 \frac{\partial \sigma_{rr}}{\partial r} + r\left(\sigma_{rr} - \sigma_{\theta\theta}\right)\right] dr = 0$$

$$\int_{R_f}^{R_\ell} \left[R_\ell^2 \frac{\partial \sigma_{rr}}{\partial r} + \frac{R_\ell^2}{r}\left(\sigma_{rr} - \sigma_{\theta\theta}\right)\right] dr = 0$$

By partial integration this system becomes

$$-\int_{R_f}^{R_\ell} r\left(\sigma_{rr}+\sigma_{\theta\theta}\right)dr+\left[r^2\sigma_{rr}\right]_{R_f}^{R_\ell}=0$$

$$\int_{R_f}^{R_\ell}\frac{R_\ell^2}{r}\left(\sigma_{rr}-\sigma_{\theta\theta}\right)dr+R_\ell^2\left[\sigma_{rr}\right]_{R_f}^{R_\ell}=0$$

This system represents the equilibrium condition (6). To this system we add the equilibrium condition in the z-direction, i.e. equation (7). Since σ_{zf} and σ_{zm} are constant, we obtain:

$$\int_{R_f}^{R_\ell}\sigma_{zz}rdr+\frac{R_f^2}{2}\sigma_{zf}+\left(\frac{R_m^2}{2}-\frac{R_\ell^2}{2}\right)\sigma_{zm}=0$$

We now define the following matrix notations, which are suitable for numerical analysis.

$$\left\{\varepsilon_\ell\right\}=\begin{bmatrix}\varepsilon_{r\ell}\\ \varepsilon_{\theta\ell}\\ e_z\end{bmatrix}=\begin{bmatrix}1 & -(R_\ell/r)^2 & 0\\ 1 & (R_\ell/r)^2 & 0\\ 0 & 0 & 1\end{bmatrix}\begin{bmatrix}c_\ell\\ D_\ell\\ e_z\end{bmatrix}=[B]\{e\}$$

$$\left\{\sigma_\ell\right\}=\begin{bmatrix}\sigma_{r\ell}\\ \sigma_{\theta\ell}\\ \sigma_{z\ell}\end{bmatrix}$$

The system of 3 equations of equilibrium can be rewritten as:

$$\{\mathcal{F}(\mathbf{e})\} = \int_{R_f}^{R_\ell} [\mathbf{B}]^T \{\sigma_\ell\} r dr + \begin{bmatrix} R_f^2 \sigma_{rf}(R_f) - R_\ell^2 \sigma_{rm}(R_\ell) \\ R_\ell^2 \sigma_{rf}(R_f) - R_\ell^2 \sigma_{rm}(R_\ell) \\ \frac{R_f^2}{2}\sigma_{zf} + \left(\frac{R_m^2}{2} - \frac{R_\ell^2}{2}\right)\sigma_{zm} \end{bmatrix} = \{0\}$$

where the upper index T denotes the transposition.

The stresses $\{\sigma_\ell\}$ are implicit function of $\{\mathbf{e}\}$ and the stresses σ_{rf}, σ_{zf}, σ_{rm} and σ_{zm} are explicit functions of $\{\mathbf{e}\}$. Then, the last system is nonlinear system of 3 equations and 3 unknowns which are the components of $\{\mathbf{e}\}$. This method looks like a FEM with only 3 DOF (degrees of freedom), which makes it a particularly efficient tool.

We introduce the following matrix notations:

$$\{U_\ell\} = \begin{bmatrix} U_\ell \\ 0 \\ ze_z \end{bmatrix} = \begin{bmatrix} r & \frac{R_\ell^2}{r} & 0 \\ 0 & 0 & 0 \\ 0 & 0 & z \end{bmatrix} \begin{bmatrix} c_\ell \\ D_\ell \\ e_z \end{bmatrix} = [\mathbf{N}]\{e\}$$

$$\{F_f\} = \begin{bmatrix} -\sigma_{rf}(R_f) \\ 0 \\ 0 \end{bmatrix}, \quad \{F_m\} = \begin{bmatrix} \sigma_{rm}(R_\ell) \\ 0 \\ 0 \end{bmatrix}, \quad \{F_z\} = \begin{bmatrix} 0 \\ 0 \\ \frac{R_f^2}{2}\sigma_{zf} + \left(\frac{R_m^2}{2} - \frac{R_\ell^2}{2}\right)\sigma_{zm} \end{bmatrix}$$

where $\{\mathbf{F}_f\}$ and $\{\mathbf{F}_m\}$ designate the external surface forces applied to the layer due to its contact with the fiber and the matrix.

With these notations, the equilibrium equations can be rewritten again as:

$$\{\mathcal{F}(\mathbf{e})\} = \int_{R_f}^{R_\ell} [\mathbf{B}]^T \{\sigma_\ell\} r dr - R_f [\mathbf{N}(R_f)]^T \{\mathbf{F}_f\} - R_\ell [\mathbf{N}(R_\ell)]^T \{\mathbf{F}_m\} + \{\mathbf{F}_z\} = \{0\}$$

It is easily shown that other forms of the strains in (ℓ) can be assumed, with the corresponding expressions of [B] and [N] being substituted into the last equation.

1.2 Iterative Approximation of the Total Strain Increment in the Layer

Keeping the previous notations, we have $\{\Delta\varepsilon_\ell\} = [\mathbf{B}]\{\Delta\mathbf{e}\}$.

- For the starting iteration, $\{\Delta\mathbf{e}\} = \{\mathbf{0}\}$ is proposed.
- If the solution found in (f), (ℓ) and (m) does not satisfy the equilibrium equations, the Newton method is used in order to propose another approximation for $\{\Delta\mathbf{e}\}$:

$$\{\mathcal{F}(\mathbf{e})\} + \left[\frac{\partial \mathcal{F}}{\partial \mathbf{e}}\right]\{\mathbf{C_e}\} = \{\mathbf{0}\}$$

where $\{\mathbf{C_e}\}$ means a "correction" to $\{\Delta\mathbf{e}\}$ and

$$\left[\frac{\partial \mathcal{F}}{\partial \mathbf{e}}\right] = \int_{R_f}^{R_\ell} [\mathbf{B}]^T [\mathbf{H}][\mathbf{B}] r dr + [\mathbf{h}^+]$$

where [H] is the "tangent" modulus in each point of (ℓ). If perfect plasticity associated with a von Mises yield surface is considered, and if the material properties are assumed not to change with temperature, then the "continuum" expression of the tensor **H** during plastic yielding is

$$\mathbf{H} = \mathbf{E}_\ell - \frac{3\mu_\ell}{\sigma_{y\ell}^2} \sigma_\ell^D \otimes \sigma_\ell^D$$

where E_ℓ is the Hooke's operator in (ℓ) and σ_ℓ^D is the deviatoric stress tensor in (ℓ).

The details of the computation of the matrix $[h^+]$ are given in Appendix A. This matrix takes into account the fact that the external loads applied to (ℓ) are not given constant, but depend on $\{e\}$.

1.3 Stresses in the Layer

Once $\{\Delta e\}$ is given, one knows $\{\Delta \varepsilon_\ell\}$ everywhere in (ℓ). The stresses (and the plastic strains) are then computed by integrating the constitutive equations. The method used is an elastic predictor/plastic correction one. A fully implicit scheme is adopted and the nonlinear equations are solved by a Newton method. It was shown recently that the general procedure presented in [7] becomes particularly simple and efficient: no linear system is solved iteratively, the corrections being found explicitly [8]. The details are not given here.

2. Numerical Results of the Axisymmetric Thermal Problem

The elastic studies performed by Jansson and Leckie [4] and Doghri et al. [5] proved that a compensating interface layer with a sufficiently high CTE can reduce significantly the residual stresses in the matrix. They also show that the hoop stress in the matrix can be reduced substantially but the axial stress in the matrix is less affected by a layer. These studies pointed out that the stresses in the layer can be high enough to induce plastic yielding.

In this section, we will study the effect of a plastic layer on the previous elastic results. The numerical results given in sections 2.1, 2.2 and 2.3 were found using the method developed in Section 1.

The fiber and the matrix are defined by the following data:

- Fiber: SiC (SCS6)

  $E_f = 360$ GPa, $\nu_f = 0.17$, $\alpha_f = 4.9 \times 10^{-6}/°C$, $R_f = 70$ μm

- Matrix: Ti3Al

  $E_m = 75.2$ GPa, $\nu_m = 0.25$, $\alpha_m = 11.7 \times 10^{-6}/°C$, $\sigma_{ym} = 380$ MPa,

$R_m = 110\mu m$

The radii R_f and R_m are related to the fiber volume fraction by

$$C_f = \left(\frac{R_f}{R_m}\right)^2 \equiv 40.5\%$$

A practical optimization procedure is proposed in [5] offering a window of candidate layer materials. According to this procedure, Silver, for example, seems to be a good candidate since matrix stresses are considerably reduced.

- The propoerties of an Ag layer and the chosen thickness are
  $E_\ell = 71$ GPa, $\nu_\ell = 0.30$, $\alpha_\ell = 25.9 \times 10^{-6}/°C$, $\sigma_{y\ell} = 100$ MPa, $t_\ell = 10\mu m$

The temperature dependence of the materials properties will be taken into account in Section 2.4.

2.1 Monotonous Cooling

A monotonous cooling corresponding to a change in temperature of $\Delta T = -800°C$ was performed with the data above. The final values of stresses and strains at the inner radii are given in Tables 1 and 2, respectively.

As in [5] a reference elastic case, corresponding to a 2 cylinder model (fiber and matrix, without layer) is used to measure the changes induced by the interface layer.

Analyzing the results, the following observations can be made.

- Plasticity in the layer results in a small increase (less than 10%) of the max. Mises stress or damage stress in the matrix by comparison to the elastic layer case. This explains why the reductions in these stresses are still important:

$$\frac{\sigma_m}{\sigma_{ref}} \cong 0.50 \text{ if } (\ell) \text{ is elastic and } \frac{\sigma_m}{\sigma_{ref}} \cong 0.55 \text{ if } (\ell) \text{ is plastic}$$

The reduction in the max. hoop stress in the matrix is even more important:

$$\frac{\sigma_{\theta m}}{\sigma_{\theta ref}} = 0.37 \text{ if } (\ell) \text{ is elastic and } \frac{\sigma_{\theta m}}{\sigma_{\theta ref}} = 0.22 \text{ if } (\ell) \text{ is plastic}$$

- When the layer is added, all the stresses in the matrix are reduced, but one notices that:

- Without the layer, the max. tensile stress in the matrix is the hoop stress $\left(\frac{\sigma_{zm}}{\sigma_{\theta m}} = 0.84\right)$

- With the layer, the axial stress in the matrix exceeds the max hoop stress and this trend is accentuated when plasticity in the layer is taken into account:

$$\frac{\sigma_{zm}}{\sigma_{\theta m}} = 1.79 \text{ if } (\ell) \text{ is elastic and } \frac{\sigma_{zm}}{\sigma_{\theta m}} = 3.46 \text{ if } (\ell) \text{ is plastic}$$

- Since the stresses in (ℓ) are reduced when plastic yielding is considered, there must be an increase in stresses elsewhere. We see that the stresses in (f) decrease and that σ_{rm} and $\sigma_{\theta m}$ decrease, then it is to be expected that σ_{zm} increases, by comparison with the elastic layer situation.

- One observes that when the layer is added, the matrix does not yield. So the assumption which was made at the beginning of this part of the study (elastic matrix) is legitimate.

- We have mentioned at the beginning of Section 1 that our solution does not verify the continuity of the stress vector at the interfaces (f)/(ℓ) and (ℓ)/(m). But the

following results show that the jumps in σ_{rr} are not too important.

$$\begin{cases}\sigma_{rr}(R_f) = -43.57\,\text{MPa} \\ \sigma_{r\ell}(R_f) = -36.27\,\text{MPa}\end{cases} \qquad \begin{cases}\sigma_{r\ell}(R_\ell) = -36.03\,\text{MPa} \\ \sigma_{rm}(R_\ell) = -30.41\,\text{MPa}\end{cases}$$

- Table 2 gives the strains in (f), (ℓ) and (m). It can be noticed that even when (ℓ) is considered elastic only, the strains in (ℓ) are important (due to high thermal strains). When we consider plasticity in (ℓ) the trend becomes accentuated (because the stresses in (ℓ) are reduced).

2.2 Sensitivity Study

Under a monotonous cooling of ΔT = -800°C, the influence of two layer parameters was studied.

a) The effect of the variation of the layer thickness was considered, all the other parameters being kept constant. The two cases: (ℓ) elastic and (ℓ) plastic were studied.

Figure 2 shows that if $\frac{t_\ell}{R_f} \leq 0.11$, the two cases give the same values of the max. Mises stress in the matrix. If $\frac{t_\ell}{R_f} > 0.11$ then for a given thickness, the max. Mises stress in the matrix is higher when the layer is plastic.

Best reductions in the max. Mises stress are:

$$\frac{\bar{\sigma}_m}{\bar{\sigma}_{ref}} \cong \begin{cases}0.5 \text{ when } (\ell) \text{ is plastic, and it is obtained for } \frac{t_\ell}{R_f} \cong 0.16 \\ 0.4 \text{ when } (\ell) \text{ is elastic, and it is obtained for } \frac{t_\ell}{R_f} \cong 0.23\end{cases}$$

The same conclusions apply for the damage equivalent stress.

b) The effect of the variation of the layer yield stress was considered, all the other parameters being kept constant. Since Mises stress = yield stress in (ℓ) (perfect plasticity), one knows that if $\sigma_{y\ell}$ increases then the stresses in (ℓ) increase and one expects that this may reduce the stresses in the matrix. But Fig. 3 shows that the value of $\sigma_{y\ell}$ does not affect the Mises stress in the matrix. However, this result leads to another interesting prediction: if the temperature dependence of properties is taken into account, plasticity in the layer will indeed occur sooner (since $\sigma_{y\ell}$ will be smaller) but the matrix will not yield and the results will not change too much. This will be checked in Section 2.4.

2.3 Thermal Cycling

To gain a preliminary idea on how the composite behaves under thermal cycling, a linear temperature history (ranging between T_1 = 825°C and T_2 = 25°C) has been considered. The results of only 3 cycles will be presented because it was found that the composite has almost shaken down after 3 cycles for the given temperature amplitude. A more complete study of the shakedown of the composite will be presented in Section 3.3. The materials data are those given at the beginning of Section 2.

The mechanical strain is defined by:

$$\varepsilon_{ij}^{MEC} = \varepsilon_{ij} - \alpha\Delta T\delta_{ij}, \quad \begin{cases} \delta_{ij} = 1 \text{ if } i = j \text{ and} \\ \delta_{ij} = 0 \text{ if } i \neq j \end{cases}$$

Figure 4a shows that during all the loading history the axial stress in the matrix exceeds the max hoop stress and is equal to the max Mises stress. Both the axial stress and max hoop stress remain tensile during the cycles. It can be seen from Fig. 4b that the axial mechanical strain in the matrix also exceeds the max hoop mechanical strain, but their values remain small.

Figure 5a shows the stress-strain response in the tangential direction at the inner radius of the interface layer. It was found that the values of the hoop stress and axial stress in the layer are almost identical. Figure 5b shows that the axial mechanical strain and the

hoop mechanical strain have almost the same values also.

2.4 Temperature Dependence of the Materials Properties

In this part of the study, the temperature dependence of the materials properties is taken into account.

The following materials were considered:

Fiber: SCS6, Matrix: Ti_3Al and Layer: Ag

The materials parameters were compiled from Ref. [9] to [13]. The fiber is elastic and the layer and the matrix are assumed to be elastic-perfectly plastic. The data are given in Figs. 6a-d.

The finite element package ABAQUS [14] was used. The F.E. mesh used for the 3 (or 2) cyclinder models is given in Fig. 7a. A generalized plane strain assumption is made. More details about the boundary conditions and the modelization are given in Appendix B.

A monotonous uniform cooling $\Delta T = -800°C$ was applied in each of the two cases: 2 cylinder model (reference case) and 3 cylinder model. Let us recall that in the previous sections, the reference case was considered to be elastic. The final values of stresses and strains at the inner radii of each material are given in Tables 3 and 4. These results show that:

- in the reference case (fiber and matrix) the matrix yields. The addition of the layer avoids yielding in the matrix.
- the layer does reduce the hoop stress in the matrix, and this reduction is important $\frac{\sigma_{\theta m}}{\sigma_{\theta ref}} = 0.23$.

It is remarkable to notice that the reduction in the hoop stress (with the same value) as well as the fact that the axial stress in the matrix exceeds the max hoop stress were observed in the previous part of this study when the temperature dependence of the materials properties has not been taken into account. One also notices that the values of the strains are almost identical to those obtained in the previous part. We may conclude that, from a qualitative point of view, taking into account the plasticity in the layer is more

important than the temperature dependence of the materials properties.

Figure 8a shows that the addition of the interface layer reduces the max Mises in the matrix and avoids plasticity to occur in the matrix. Fig. 8b shows that the interface layer can reduce dramatically the max hoop stress in the matrix, while the axial stress in the matrix is increased:

$$\frac{\sigma_{\theta m}}{\sigma_{\theta ref}} = 0.23 \text{ and } \frac{\sigma_{zm}}{\sigma_{zref}} = 1.42$$

3. Thermal-Mechanical Computations for a Hexagonal Array of the Composite

The manufacture and testing of composite materials is demanding in time and effort so that there is special need for procedures which can help determine the macroscopic properties of the materials from the properties of the constituents. Success in this endeavor would mean that prediction of composite properties would bypass expensive and time-consuming manufacture and test procedures.

The so-called homogenization procedure is used to predict the macroscopic properties of the composite from the properties of the individual constituents.

The composite under consideration is composed of a hexagonal array of SCS6 fibers coated with the interface layer, in a Ti_3Al matrix (Fig. 9). A hexagonal array presents more symmetries then a square array. Taking into account the structure periodicity, the problem can be reduced, for symmetric loadings, to the study of a single unit cell (ODBA), shown in Fig. 9, with the appropriate boundary conditions, as detailed in Appendix B.

Resuls for the unit cell under thermal loading only will allow to appreciate the validity of the 3 cylinder model used earlier. With the unit cell, it will be also possible to study the composite behavior under transverse mechanical loading since the 3 cylinder model is clearly not adequate for non-axisymmetric problems. The study was conducted using ABAQUS [14]. The F.E. mesh for the cell is shown in Fig. 7b.

The matrix and the interface layer are assumed to be elastic-perfectly plastic, while the fiber remains elastic. The materials properties of the 3 materials are temperature dependent.

3.1 Monotonous Cooling

A monotonous uniform cooling (ΔT = -800°C) was applied to the unit cell. The resulting values of stresses and strains were found to be almost identical to those obtained for the 3 cylinder model, and presented in section 2.4. So, for axisymmetric problems, the 3 cylinder model seems to be a simple but accurate representation.

3.2 First yield points in the matrix

Several proportional monotonously increasing thermal-mechanical loadings were applied to the unit cell. The mechanical loading is an average stress Σ_{11} corresponding to a macroscopic uniaxial stress state in the 1-direction ($\Sigma_{11} \neq 0$, $\Sigma_{ij} = 0$ if $i \neq 1$ or $j \neq 1$). The initial temperature is $T_0 = 25°C$, and two initial stress states were considered:

- no initial residual stresses,
- initial residual stresses due to a cooling down from

  $T_i = 825°C$ to $T_0 = 25°C$

The points of first yield in the matrix for each case are reported in Fig. 10. The results show that the residual stresses offer a reserve of elasticity to the matrix and the composite.

3.3 Shake down

Thermal cycling is applied to the composite under a constant macroscopic stress Σ_{11} in the 1-direction. Shake down is obtained when the macroscopic strain keeps the same value at the end of each cycle. Limit shake down points are reported in Fig. 10 .

In excess of the shake down limit values, the composite rachets on each cycle of thermal loading. Inside the shake down region, the composite behaves elastically. The results of Fig. 10 show that the particular interface layer (Ag) considered as an example in this work does not extend the temperature range for shake down in the composite. The reason is that the yield stress of this layer is too low. As pointed out in [4], to improve the low cycle fatigue of the composite, it is desirable to have a layer with a high yield stress.

CONCLUSIONS

The optimization procedure proposed in [5] on the basis of an elastic study allows to have good candidate layer materials. The elasto-plastic analysis conducted here confirms that such interface layers can reduce the hoop stress and the v. Mises equivalent stress in the matrix significantly. However, the axial stress in the matrix is less affected by a layer (and it may even increase). This implies that these layers could be successful in composites where predominatly radial cracking is observed in the matrix. The interface layer should be ductile enough to sustain relatively high strains. It should also have a yield stress high enough to improve the range of shake down of the composite.

It appears that taking into account plasticity is much more important than the temperature dependence of the materials properties. Comparison between the results given by the 3 cylinder model and a unit cell of a hexagonal array shows that for axisymmetric problems the concentric cylinder is a simple but accurate model.

ACKNOWLEDGEMENT

The work was supported by a grant from the NASA-Lewis Research Center. The authors wish to express their gratitude to Dr. Steve Arnold for the encouragement and support.

REFERENCES

[1] Brindley, P.K., Bartolotta, P.A. and MacKay, R.A., "Thermal and Mechanical Fatigue of SiC/Ti_3Al+Nb," 2nd HITEMP Review, NASA CP-10039, paper 52, 1989.

[2] Ghosn, L.J. and Bradley, A.L., "Optimum Interface Properties for Metal Matrix Composites," NASA TM-102295, 1989.

[3] Caruso, J.J., Chamis, C.C. and Brown, H.C., "Parametric Studies to Determine the Effects of Compliant Layers on Metal Matrix Composite Systems," NASA TM-102465, 1990.

[4] Jansson, S. and Leckie, F.A., "Reduction of Thermal Stresses in Continuous Fiber Reinforced Metal Matrix Composites with Interface Layers," submitted for publication, 1990.

[5] Doghri, I., Jansson, S., Leckie, F.A. and Lemaitre, J., "Optimization of Interface Layers in the Design of Ceramic Fiber Reinforced Metal Matrix Composites," submitted for publication, 1990.

[6] Lemaitre, J. and Chaboche, J.L., Mechanics of Solid Materials, Cambridge University Press, 1990.

[7] Benallal, A., Billardon, R. and Doghri, I., "An Integration Algorithm and the Corresponding Consistent Tangent Operator for Fully Coupled Elasto-Plastic and Damage Equations," Comm. Appl. Numer. Meth., 4, 731-740, 1988.

[8] Lematire, J. and Doghri, I., "DAMAGE 90: A Post Processor for Crack Initiation," submitted for publication, 1990.

[9] Brindley, P.K., Draper, S.L., Nathal, M.V. and Eldridge, J.I., "Factors which Influence Tensile Strength of SiC/Ti_3Al+Nb," 2nd HITEMP Review, NASA CP-10039, paper 51, 1989.

[10] Shafrik, R.E., "Dynamic Elastic Moduli for the Titanium Aluminides," Metall. trans. A, Vol. 8A, pp. 1003-1006, June 1977.

[11] Dicarlo, J.A., "High Temperature Properties of CVD Silicon Carbide Fibers," Int. Conf. of Whisher- and Fiber-Toughened Ceramics, Oak Ridge, Tennessee, June 7-9, 1988.

[12] Jansson, S., Déve, H.E. and Evans, A.G., "The Anisotropic Mechanical Properties of a Ti Matrix Composite Reinforced with SiC Fibers," UCSB, College of Engineering of Engineering, to be published, 1990.

[13] Boyer, H.E. and Gall, T.L., Metal Handbook, Desk Edition, ASM Metal Park, 1985.

[14] ABAQUS, Hibbit, Karlsson and Sorensen, Inc., version 4.7.

[15] Ranaweera, M.P., "Finite Element Analysis of a Metal Matrix Composite Under Mechanical and Thermal Loading," Report, UCSB, Dept. of Mech. Eng., June 1989.

APPENDIX A. Stresses in (f) and (m) and contributions of (f) and (m) to the incremental stiffness matrix.

The fiber and the matrix being assumed here to be elastic, their strain and stress fields are completely defined by the knowledge of 3 constants: c_f, c_m, D_n (see [5]).

The solution in (f) is found by solving eqn. (3):

$$c_f R_f = c_\ell R_f + D_\ell \frac{R_\ell^2}{R_f} \Rightarrow c_f = c_\ell + \left(\frac{R_\ell}{R_f}\right)^2 D_\ell$$

The radial and longitudinal stresses in (f) at $r = R_f$ are then:

$$\sigma_{rf} = 2(\lambda_f + \mu_f)c_f + \lambda_f e_z - (3\lambda_f + 2\mu_f)\alpha_f \Delta T$$

$$\sigma_{zf} = 2\lambda_f c_f + (\lambda_f + 2\mu_f)e_z - (3\lambda_f + 2\mu_f)\alpha_f \Delta T$$

The solution in (m) is found by solving eqn. (4) and (5):

- $$c_m R_\ell + \frac{R_m^2}{R_\ell} D_m = c_\ell R_\ell + D_\ell R_\ell$$

$$\Rightarrow \quad c_m + \left(\frac{R_m}{R_\ell}\right)^2 D_m = c_\ell + D_\ell$$

- $$2(\lambda_m + \mu_m)c_m + \lambda_m e_z - 2\mu_m D_m - (3\lambda_m + 2\mu_m)\alpha_m \Delta T = 0$$

That gives

$$D_m = \frac{\lambda_m e_z + 2(\lambda_m + \mu_m)(c_\ell + D_\ell) - (3\lambda_m + 2\mu_m)\alpha_m \Delta T}{2\mu_m + 2(\lambda_m + \mu_m)\left(\frac{R_m}{R_\ell}\right)^2}$$

and $$c_m = c_\ell + D_\ell - \left(\frac{R_m}{R_\ell}\right)^2 D_m$$

Then, the radial and longitudinal stresses in (m) at $r = R_\ell$ are

$$\sigma_{rm} = 2(\lambda_m + \mu_m)c_m + \lambda_m e_z - 2\mu_m\left(\frac{R_m}{R_\ell}\right)^2 D_m - (3\lambda_m + 2\mu_m)\alpha_m \Delta T$$

$$\sigma_{zm} = 2\lambda_m c_m + (\lambda_m + 2\mu_m)e_z - (3\lambda_m + 2\mu_m)\alpha_m \Delta T$$

Computation of $[\mathbf{h}^+]$

The matrix $[\mathbf{h}^+]$ contains the partial derivatives of the stresses σ_{rf}, $\sigma_{rm}(R_\ell)$, σ_{zf} and σ_{zm} with respect to the components (c_ℓ, D_ℓ and e_z) of {e} (see Sections 1.1 and 1.2).

- Fiber contribution

We have

$$\frac{\partial c_f}{\partial c_\ell} = 1, \quad \frac{\partial c_f}{\partial D_\ell} = \left(\frac{R_\ell}{R_f}\right)^2 \quad \text{and} \quad \frac{\partial c_f}{\partial e_z} = 0$$

$$\frac{\partial \sigma_{rf}}{\partial c_\ell} = 2(\lambda_f + \mu_f)\frac{\partial c_f}{\partial c_\ell}, \frac{\partial \sigma_{rf}}{\partial D_\ell} = 2(\lambda_f + \mu_f)\frac{\partial c_f}{\partial D_\ell}$$

$$\frac{\partial \sigma_{rf}}{\partial e_z} = 2(\lambda_f + \mu_f)\frac{\partial c_f}{\partial e_z} + \lambda_f$$

$$\frac{\partial \sigma_{zf}}{\partial c_\ell} = 2\lambda_f \frac{\partial c_f}{\partial c_\ell}, \frac{\partial \sigma_{zf}}{\partial D_\ell} = 2\lambda_f \frac{\partial c_f}{\partial D_\ell}$$

$$\frac{\partial \sigma_{zf}}{\partial e_z} = 2\lambda_f \frac{\partial c_f}{\partial e_z} + (\lambda_f + 2\mu_f)$$

- Matrix contribution:

We have

$$\frac{\partial D_m}{\partial c_\ell} = \frac{2(\lambda_m + \mu_m)}{2\mu_m + 2(\lambda_m + \mu_m)\left(\frac{R_m}{R_\ell}\right)^2} = \frac{\partial D_m}{\partial D_\ell}$$

$$\frac{\partial D_m}{\partial e_z} = \frac{\lambda_m}{2\mu_m + 2(\lambda_m + \mu_m)\left(\frac{R_m}{R_\ell}\right)^2}$$

$$\frac{\partial c_m}{\partial c_\ell} = 1 - \left(\frac{R_m}{R_\ell}\right)^2 \frac{\partial D_m}{\partial c_\ell} = \frac{\partial c_m}{\partial D_\ell}, \frac{\partial c_m}{\partial e_z} = -\left(\frac{R_m}{R_\ell}\right)^2 \frac{\partial D_m}{\partial e_z}$$

$$\frac{\partial \sigma_{rm}}{\partial c_\ell} = 2(\lambda_m + \mu_m)\frac{\partial c_m}{\partial c_\ell} - 2\mu_m\left(\frac{R_m}{R_\ell}\right)^2 \frac{\partial D_m}{\partial c_\ell} = \frac{\partial \sigma_{rm}}{\partial D_\ell}$$

$$\frac{\partial \sigma_{rm}}{\partial e_z} = 2(\lambda_m + \mu_m)\frac{\partial c_m}{\partial e_z} - 2\mu_m\left(\frac{R_m}{R_\ell}\right)^2 \frac{\partial D_m}{\partial c_\ell} + \lambda_m$$

$$\frac{\partial \sigma_{zm}}{\partial c_\ell} = 2\lambda_m \frac{\partial c_m}{\partial c_\ell} = \frac{\partial \sigma_{zm}}{\partial D_\ell}$$

$$\frac{\partial \sigma_{zm}}{\partial e_z} = 2\lambda_m \frac{\partial c_m}{\partial e_z} + (\lambda_m + 2\mu_m)$$

APPENDIX B. Modelization and Finite Element Discretization

(a) Two and Three Cylinder Models

Because of the symmetry of the problem, only a quarter of the cross section is considered. The dimensions and the mesh used are shown in Fig. 7a. ABAQUS generalized plane strain elements CGPE6 and CGPE5 were used, two extra nodes (EX1 and EX2) are needed to impose the generalized plane strain condition. The node EX1 has one degree of freedom (DOF) representing the longitudinal displacement which is the increase in thickness of the model. The node EX2 takes care of the rotations of the end planes, and these are prescribed to be zero.

The normal displacements of the nodes of the 2 straight edges of the section in Fig. 7a are imposed to be zero. The two cylinder model (fiber and matrix) is simply obtained by saying that the layer material is identical to the matrix one.

(b) Unit Cell

The composite is composed of a hexagonal array of SCS6 fibers coated with the interface layer, in a Ti_3Al matrix. The transverse section is given in Fig. 9. The following approach considered in [15] was kept in this study.

Edge effects will not be considered in this study, and hence the analysis can be done using the theory of homogenization. We consider symmetric loading such that the edges of the unit cell as well as the axes 01 and 02, will remain straight during deformation. Hence only a quarter of the unit cell need to be considered for analysis, and this is taken to be the positive quadrant of the 01,2 axes.

If this quarter cell (OFEA) is isolated and allowed to deform symmetrically,it will undergo displacements as shown in Fig. 11a. The centerline DCB, about which the region is skew-symmetric, will displace as shown. If (Cu1, Cu2) are the displacements of C, (Pu1, Pu2) are the displacements of a point P on CB, and (Qu1, Qu2) are the displacements of a point Q on DC such that QC = CP, then:

$Cu1 = Cu2 = 0,$

$Pu1 + Qu1 = 0$, and

$Pu2 + Qu2 = 0$

If this skew-symmetry is taken into account, only the half (ODBA) of the quarter cell need to be analyzed. The deformed shape of (ODBA) is shown in Fig. 11b, after giving it a rigid body translation so that points in the side OD do not undergo u2 displacements.

In analyzing the region (ODBA), the boundary conditions to be used are:

i. Along OD, $u2 = 0$

ii. Along OA, $u1 = Au1$

iii. Along BA, $u2 = Au2$

iv. Along DB, for points such as P and Q,

$Pu1 + Qu1 = 0$

$Pu2 + Qu2 = Au2$

The finite element mesh used is given in Fig. 7b. The type of elements is the same as in section (a).

With the boundary conditions given earlier, the key displacements of the F.E. model are the u1 and u2 displacements of the node A and the u3 displacement of the extra node EX1. In terms of these nodal displacements, the average (macroscopic) direct strains in the composite are given by:

$$\varepsilon_{11} = -\frac{u1(A)}{\frac{\sqrt{3}}{2}h}, \quad \varepsilon_{22} = \frac{u2(A)}{h}, \quad \varepsilon_{33} = \frac{u3(EX1)}{1}$$

a unit longitudinal thickness being considered.

Stresses in Matrix

Stress		rr	θθ	zz	Mises $\bar{\sigma}$	Damage σ^*
Ref.	σ (MPa)	-187.3	442.2	372.0	597.5	602.5
(ℓ)	σ (MPa)	-50.4	163.5	292.8	300.2	320.3
elastic	σ/σ_{ref}	0.27	0.37	0.79	0.50	0.53
(ℓ)	σ (MPa)	-30.4	98.7	342.0	327.5	342.7
plastic	σ/σ_{ref}	0.16	0.22	0.92	0.55	0.57

Stresses in Layer

Stress		rr	θθ	zz	Mises	Damage
(ℓ) elastic	σ (MPa)	-260.1	1529.5	1437.1	1745.2	1901.7
(ℓ) plastic	σ (MPa)	-36.3	64.9	62.5	100.0	98.8

Stresses in Fiber

Stress		rr	θθ	zz	Mises	Damage
Ref.	σ (MPa)	-187.3	-187.3	-546.5	359.3	536.0
(ℓ) elastic	σ (MPa)	-260.1	-260.1	-780.5	520.4	763.8
(ℓ) plastic	σ (MPa)	-43.6	-43.6	-417.8	374.2	406.6

Table 1. Stresses at the Inner Radii of the Compound Cylinder after Monotonous Cooling (Materials properties given at room temperature)

Strains in MATRIX

Strains		rr	θθ	zz
Reference	ε (%)	-1.45	-0.41	-0.52
(ℓ) elastic	ε (%)	-1.15	-0.80	-0.58
(ℓ) plastic	ε (%)	-1.12	-0.90	-0.50

Thermal strains: $\alpha_m \Delta T = -0.94\%$

Strains in LAYER

Strains		rr	θθ	zz
(ℓ) elastic	ε (%)	-3.69	-0.41	-0.58
	ε (%)	-5.27	-0.38	-0.50
(ℓ) plastic				
	ε^p (%)	3.10	1.60	1.50

Thermal strains: $\alpha_\ell \Delta T = -2.07\%$

Strains in FIBER

Strains		rr	θθ	zz
Reference	ε (%)	-0.41	-0.41	-0.53
(ℓ) elastic	ε (%)	-0.41	-0.41	-0.58
(ℓ) plastic	ε (%)	-0.38	-0.38	-0.50

Thermal strains: $\alpha_f \Delta T = -0.39\%$

Table 2. Strains at the Inner Radii of the Compound Cylinder after Monotonous Cooling (Materials properties given at room temperature)

Stresses in Matrix

Stress		rr	θθ	zz	Mises $\bar{\sigma}$	Damage σ^*
Reference	σ (MPa)	-130.8	261.7	235.4	380.0	377.7
3 cylinder	σ (MPa)	-13.43	61.82	335.0	317.5	329.3
model	σ/σ_{ref}	0.10	0.23	1.42	0.83	0.87

Stresses in Layer

Stress		rr	θθ	zz	Mises	Damage
3 cylinder	σ (MPa)	-1.40	98.13	99.07	100.0	117.4

Stresses in Fiber

Stress		rr	θθ	zz	Mises	Damage
Reference	σ (MPa)	-159.7	-159.7	-503.7	344.0	491.3
3 cylinder	σ (MPa)	-41.18	-41.18	-426.7	385.5	415.8
model	σ/σ_{ref}	0.26	0.26	0.85	1.12	0.84

Table 3. Stresses at the Inner Radii of the Compound Cylinder after Monotonous Cooling (temperature dependence of materials properties taken into account)

Strains in MATRIX

Strain (%)	ε_{rr}	$\varepsilon_{\theta\theta}$	ε_{zz}	Accumulated plastic strain
Reference	-1.61	-0.437	-0.517	0.34
3 cylinder	-1.08	-0.961	-0.506	0

Strains in LAYER

Strain (%)	ε_{rr}	$\varepsilon_{\theta\theta}$	ε_{zz}	Accumulated plastic strain
3 cylinder	-5.00	-0.594	-0.506	2.94

Strains in FIBER

Strain (%)	ε_{rr}	$\varepsilon_{\theta\theta}$	ε_{zz}
Reference	-0.405	-0.405	-0.517
3 cylinder	-0.381	-0.381	-0.506

Table 4. Strains at the Inner Radii of the Compound Cylinder after Monotonous Cooling (temperature dependence of materials properties taken into account)

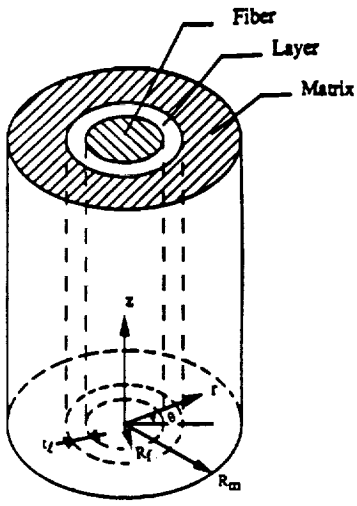

Figure 1.—Concentric 3 cylinder model.

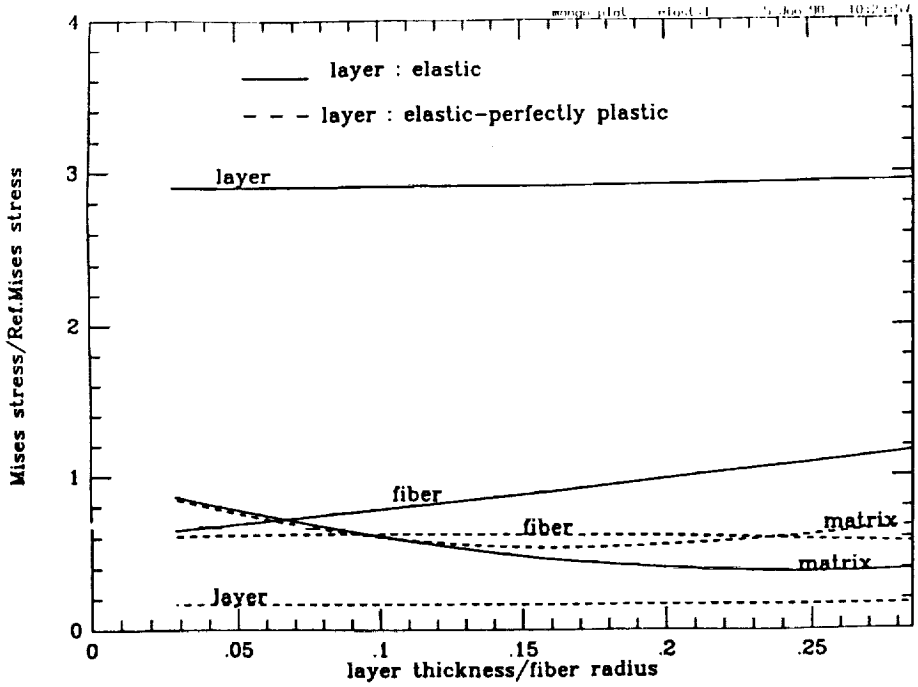

Figure 2.—Influence of the layer thickness on the max Mises stress in the matrix.

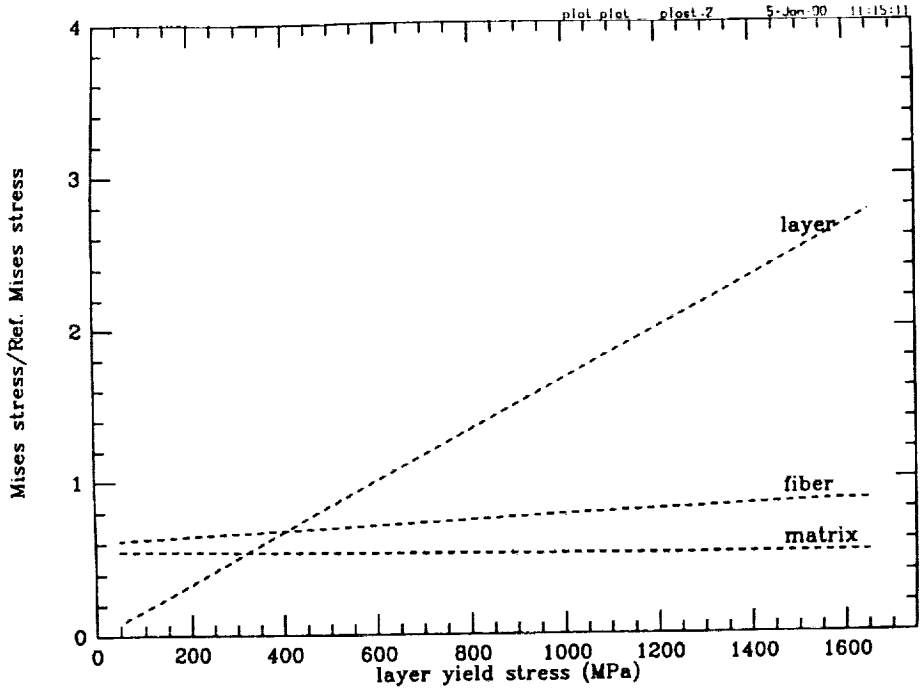

Figure 3.—Influence of the layer yield stress on the max Mises stress in the matrix.

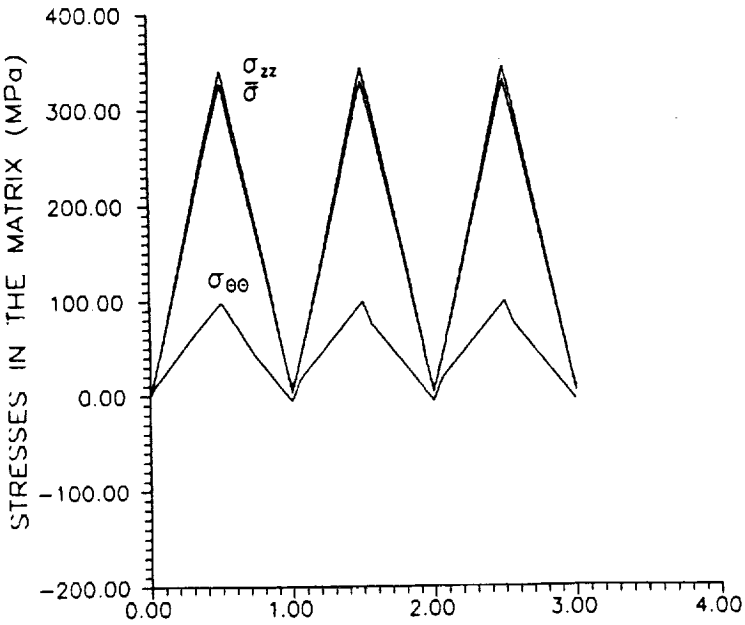

(a) Stresses.

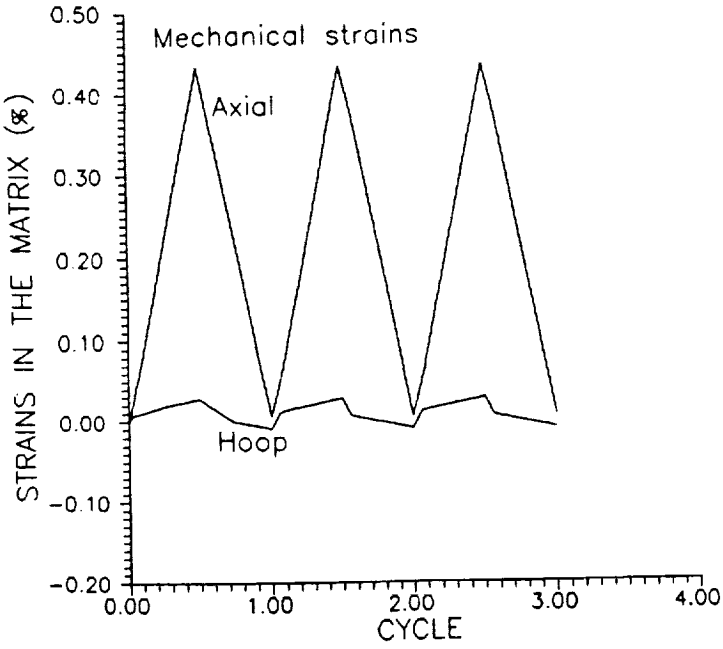

(b) Mechanical strains.

Figure 4.—Thermal cycling - history at the inner radius of the matrix cylinder.

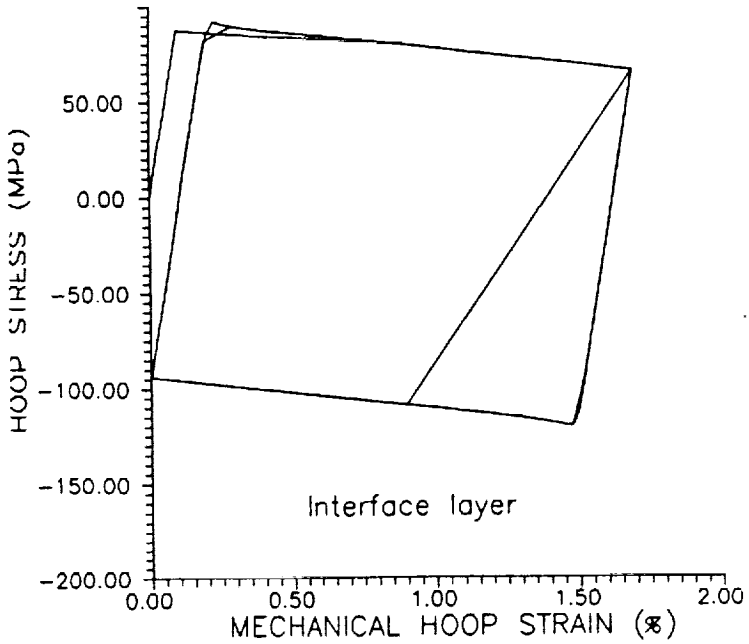

(a) Stress-strain response.

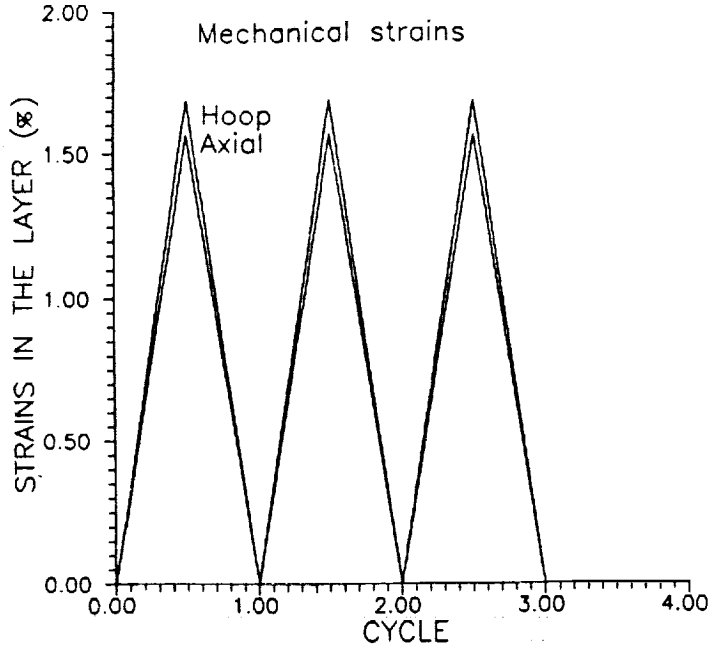

(b) History of mechanical strains.

Figure 5.—Thermal cycling at the inner radius of the layer cylinder.

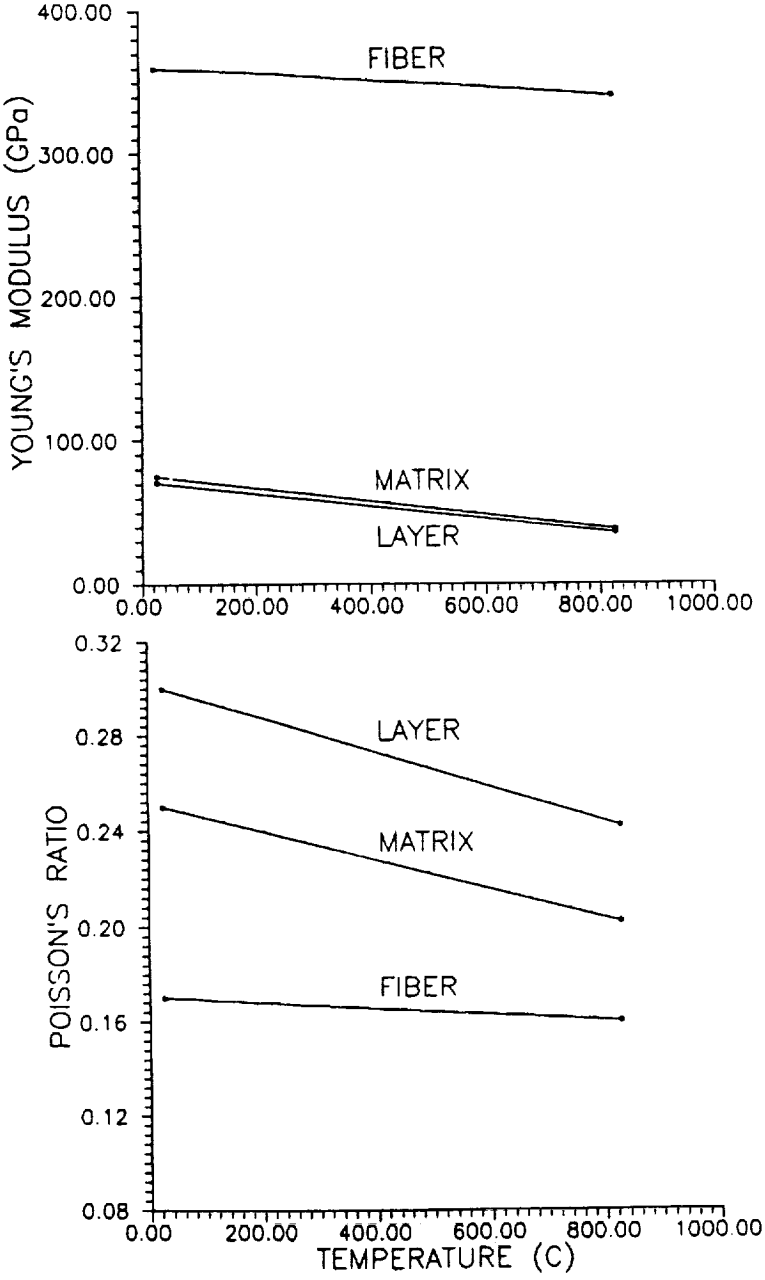

Figure 6.—Temperature dependence of the materials properties - Fiber: SiC(SCS6), Matrix: Ti_3Al, Layer: Ag.

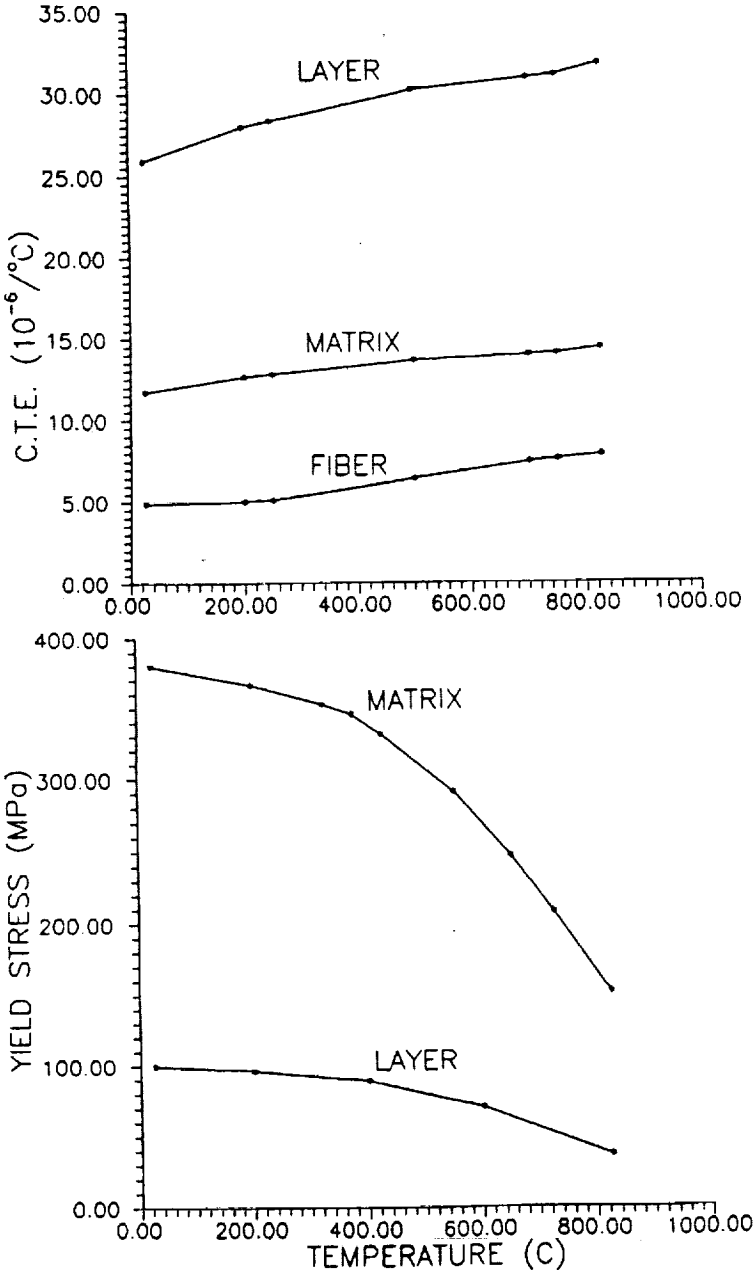

Figure 6.—Concluded.

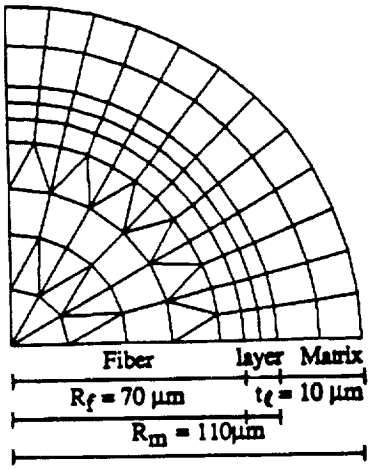

(a) Three cylinder model.

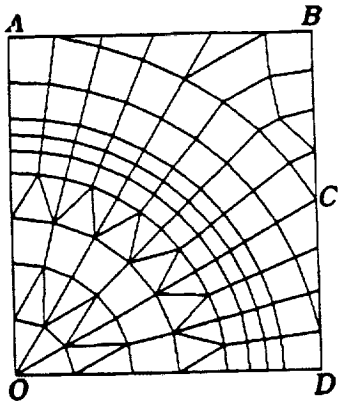

(b) Unit cell of a hexagonal array.

Figure 7.—Finite element meshes.

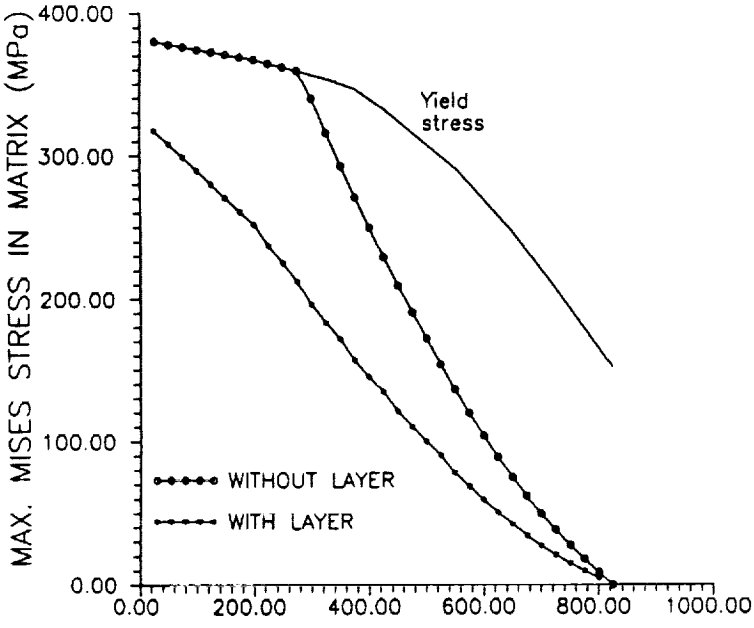

(a) v.Mises equivalent stress.

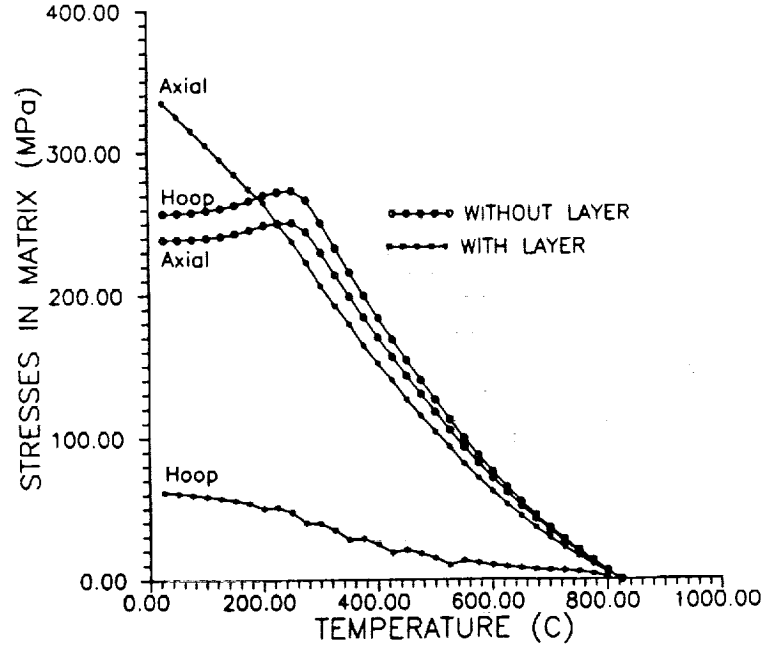

(b) Tensile stress.

Figure 8.—Cooling down - evolution of the stresses at the inner radius of the matrix cylinder.

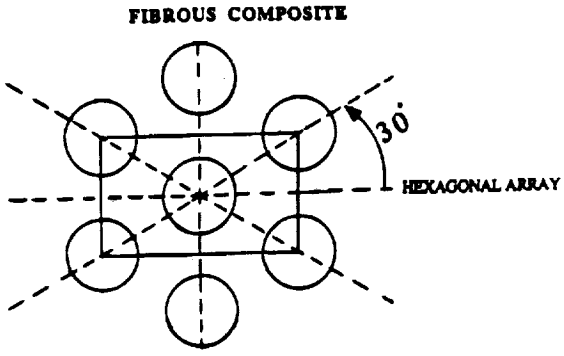

(a) Hexagonal array.

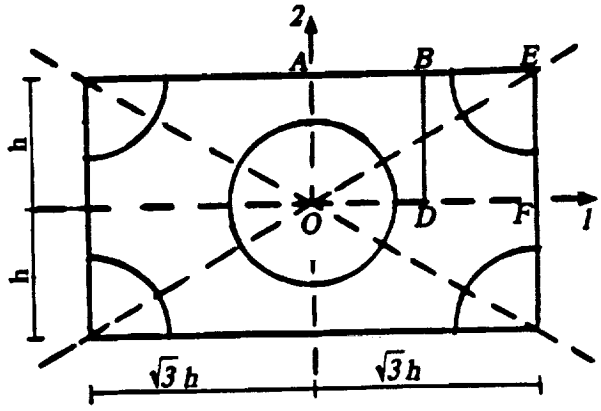

(b) Region of analysis.

Figure 9.—Fibrous composite.

Unit cell parameter: $h = \left[\frac{\pi}{2\sqrt{3}\, c_f}\right]^{1/2}$ $R_f = 104.8\ \mu m$

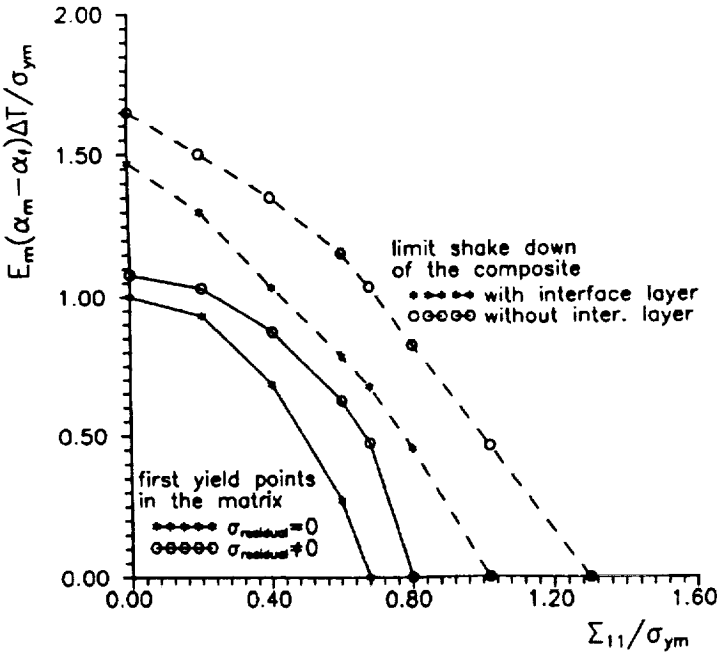

Figure 10.—First yield points in the matrix and limit points of shake down of the composite.

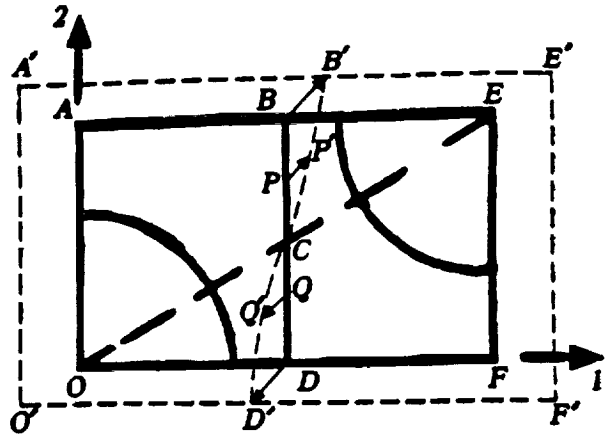

(a) Region of analysis and boundary conditions.

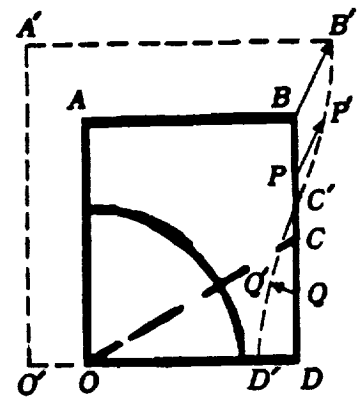

(b) Unit cell and boundary conditions.

Figure 11.—Unit cell definition.

NASA
National Aeronautics and Space Administration

Report Documentation Page

1. Report No.	2. Government Accession No.	3. Recipient's Catalog No.
NASA CR-187133		

4. Title and Subtitle
Elasto-Plastic Analysis of Interface Layers for Fiber Reinforced Metal Matrix Composites

5. Report Date
June 1991

6. Performing Organization Code

7. Author(s)
I. Doghri and F.A. Leckie

8. Performing Organization Report No.
None

10. Work Unit No.
510-01-50

9. Performing Organization Name and Address
University of California
Department of Mechanical and Environmental Engineering
Santa Barbara, California 93106

11. Contract or Grant No.
NAG3-894

13. Type of Report and Period Covered
Contractor Report
Final

12. Sponsoring Agency Name and Address
National Aeronautics and Space Administration
Lewis Research Center
Cleveland, Ohio 44135-3191

14. Sponsoring Agency Code

15. Supplementary Notes
Project Manager, Steven M. Arnold, Structures Division, NASA Lewis Research Center, (216) 433-3334.

16. Abstract
The mismatch in coefficients of thermal expansion (CTE) of fiber and matrix in metal matrix composites reinforced with ceramics fibers induces high thermal stresses in the matrix. Elasto-plastic analyses—with different degrees of simplification and modelization—show that an interface layer with a sufficiently high CTE can reduce the tensile hoop stress in the matrix substantially.

17. Key Words (Suggested by Author(s))
Thermal expansion; Elastic; Plastic deformation; Thermal stresses; Residual stresses

18. Distribution Statement
Unclassified - Unlimited
Subject Category 39

19. Security Classif. (of the report)	20. Security Classif. (of this page)	21. No. of pages	22. Price*
Unclassified	Unclassified	40	A03

NASA FORM 1626 OCT 86

*For sale by the National Technical Information Service, Springfield, Virginia 22161